Vanadium Dioxide for Reconfigurable Antennas and Microwave Devices

Dimitris E. Anagnostou, David Torres, Tarron S. Teeslink, and Nelson Sepulveda

Vanadium Dioxide for Reconfigurable Antennas and Microwave Devices

Enabling RF reconfigurability through smart materials.

We present a comprehensive study of a new method to reconfigure, tune, and/or program antennas and radio-frequency (RF) devices. The method consists of using electrical signals to induce the solid-to-solid phase transition in vanadium dioxide (VO_2) thin-film patterned structures that connect the device metallization layer with extensions, thus effectively changing the geometry of the device. Applied voltage pulses to a resistive heater electrically isolated from the antenna metallization layers increase the temperature of the VO_2 strip across the phase transition. Hence, the VO_2-biasing mechanism and the antenna are electrically decoupled, which enables an additional degree of freedom for antenna and microwave device engineers as the reconfiguration is no longer restricted by any biasing network limitations. Radiation patterns are also maintained unaffected. This decoupling adds into the design spectrum, applications that require wideband tuning, low-loss structures (e.g., arrays and reflectarrays), and even reconfigurable cloaks. The VO_2 switch is arguably the smallest ever used to reconfigure an antenna, which requires further circuit element considerations. The presented method is validated through a series of antenna prototypes that demonstrate VO_2 applicability on wire and aperture antennas. Details and challenges of the monolithic integration of VO_2 thin films and resistive heaters for reconfigurable antennas, along with the measurement setup, are presented. Results unveil this new reconfiguration technique and suggest further applications, as the VO_2 may also be activated optically.

Digital Object Identifier 10.1109/MAP.2020.2964521
Date of current version: 27 February 2020

INTRODUCTION

The phase transition of a material occurs under certain stimuli and affects the material molecular structure. An example of a common material that changes phase is water, which becomes solid, liquid, or gas at different temperatures. Interestingly, the relative dielectric permittivity of water also changes, from $\varepsilon_r = 80$ at its liquid state, to $\varepsilon_r = 3.2$ when solid, while its volume increases by 5%.

VO_2 is a phase-change material, first reported in 1959 [1], that undergoes an insulator-to-semiconductor transition when subjected to a variety of stimuli. During the transition, VO_2 exhibits orders of magnitude of change in electrical resistivity (ρ) and relative dielectric permittivity (ε_r), referred to as *insulator-to-metal transition* (*IMT*). Although VO_2 has been used in terahertz applications [2], [3], there have been very few reported antenna prototypes in the gigahertz range. This article reports results from the first exploration of the hypothesis that VO_2 can be used in reconfigurable and tunable RF devices.

The VO_2 transition occurs through various methods: conductive heating [4], Joule heating [5], using photothermal techniques [6], voltage biasing [7], and ultrafast optical excitation [8]. This work explores how convective heating and resistive heating can provide significant advantages for reconfigurable antennas and RF component applications. Traditionally, reconfigurable antennas employ electrically connected components, such as RF microelectromechanical systems (MEMS) [9]–[13], positive-intrinsic-negative (p-i-n) diodes [14], varactors [15], and field-effect transistors (FETs) [16] that are also nonlinear in nature. However, these components also demonstrate limitations in RF performance in terms of efficiency, power handling, and frequency tunability imposed by their biasing circuitry, while their integration or soldering can reduce device reliability and robustness. As an example, the FET transistor biasing network [16] shown in Figure 1 has also been used in many tunable antenna and filter designs [17]–[19]. The network limits the tuning range to about 20% or less, which is the bandwidth of the quarter-wave open-circuited stub with the quarter-wave line. Moreover, the FET transistors had to be placed near the ends of the slot at low impedance points to prevent mismatch and field changes, which imposed additional limitations on the design flexibility and thus affected the available tunable bandwidth. In another example [16], the same biasing network reconfigures a coupled lines filter at six different states, achieving a 15% tuning range.

Wideband biasing matching networks require multiple components that increase design complexity, cost, and losses. The presented technology eliminates the need for $\lambda/4$ stubs, small capacitors, and inductors that require soldering. This can prove valuable for antenna engineers. The fact that the activation mechanisms are resistive heaters that do not touch the RF/radiating structure make the VO_2 technology very advantageous.

There have also been some notable recent advances related to VO_2. Researchers investigated thermal triggering of VO_2 RF switches on tin oxide (SnO_2) and titanium oxide (TiO_2) substrates achieving more than 15-dB change in insertion loss [20]. Also, in another interesting work, Yang et al. reported an inkjet-printed VO_2 RF switch with 40-μs actuation that operates to 40 GHz and has a two orders-of-magnitude ON/OFF response [21]. Further insights into the IMT transition process were presented in [22].

However, until recently no articles in the literature discussed the bandwidth limitations of the reconfigurable antennas. These limitations motivated investigations of alternative methods to achieve reconfigurability for antenna designs. Here we show how the relatively new technology of phase-change materials can overcome bandwidth limitations by decoupling the bias network from the design, and how it can lead to larger reconfigurable structures with low loss.

The most important characteristic of the VO_2 switch is that its phase change can be actuated without electrically connecting a biasing circuit to the antenna. This characteristic can be particularly useful for antenna designers as it allows the antenna to be reconfigurable without the complexities associated with the integration of MEMS or with the soldering of passive or active off-the-shelf components. This additional degree of freedom can be obtained by integrating resistive heaters underneath the VO_2 thin films. The resistive heaters are electrically biased, but they are not electrically connected to the antenna structure or to the VO_2 thin film. The phase change is enabled through heat transfer from the heater to the VO_2 film through the material. Without any electrical coupling, the only form of coupling that can affect the design is the mutual coupling between the VO_2 films and the bias lines. These lines, however, are thin and can be designed so that their electric-field (E-field) vector near the antenna surface is perpendicular (cross-polarized) to the antenna, which practically eliminates any field disturbance due to coupling.

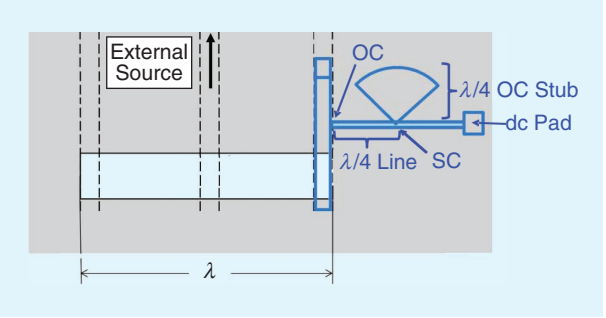

FIGURE 1. A typical example of the biasing circuit of a tunable antenna using FET transistors to alter the circumference of the one-wavelength-long slot. The biasing network (shown for one slot with blue lines) is on the back side and consists of a quarter-wave open-circuit (OC) stub connected to a quarter-wave line (adopted from [16]). The effective OC and short circuit (SC) "seen" by the current are noted. The tuning range is limited to about 15%.

VO_2 PHYSICS AND MODELING

Phase transitions, which usually occur as a function of temperature and pressure, are commonly observed as changes between the four states of matter: solid, liquid, gas, and plasma. There are, however, other types of phase transformation where for both phases the material remains a solid. Graphite and diamonds are examples of solids made of the same elements but with significant differences in their properties due to a different atom orientation or crystal structure. In these cases, going from one phase to the other involves specific combinations of high pressures and temperatures. However, there are a few solid–solid phase-change materials that only require a change in temperature, E-field, carrier injection, or ultrafast optical radiation to induce a change in the crystal orientation that comes with drastic changes in the material properties [23]. Among these types of phase-change materials, VO_2 has the phase change that is closest to room temperature, happening at about 68 °C [23].

THE BEHAVIOR AND PHYSICS OF VO_2

The first-order phase transformation in VO_2 comes with an abrupt change in the electrical, mechanical, and optical

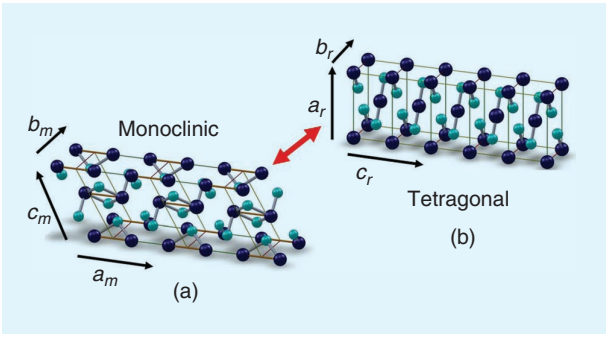

FIGURE 2. (a) Below 68 °C, the monoclinic structure of the VO_2 binds its electrons and limits its conductivity. (b) Above 68 °C, in the conducting phase, large vibrational motions (phonons) stabilize the tetragonal crystal structure (phase) and free up conduction electrons, increasing the conductivity of the material, according to [24], [25]. (Source: Wiley; used with permission.)

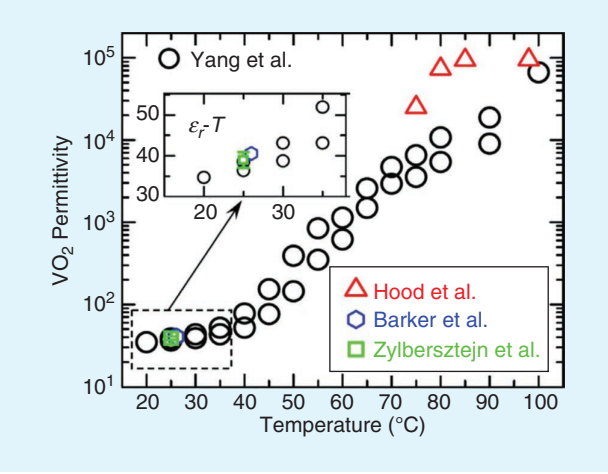

FIGURE 3. The measured relative dielectric permittivity shift of VO_2 versus temperature, indicating an increase of three orders of magnitude when the VO_2 is heated [26]. Literature values from Yang et al. [26] are also shown together for comparison with Hood et al. ([40] in [26]), Barker et al. ([42] in [26]), and Zylbersztejn et al. ([41] in [26]). (Source: American Physical Society; used with permission.)

properties of the material that shows hysteretic behavior. Crystalline VO_2 remains a crystal in both phases, with a monoclinic structure at room temperature and tetragonal structure at high temperature. The unit cell in the monoclinic phase is double the size of that in the tetragonal phase. Figure 2 shows a diagram of the crystal change in VO_2 across its phase transition. The VO_2 exhibits an abrupt change in the resistance of VO_2 across its phase transformation—where the material shows about a three-order drop in resistance during its monoclinic → tetragonal crystallographic change. This transition is typically referred to as an *IMT*.

To assist in electromagnetic designs, it is useful to have estimates of the VO_2 material properties, specifically the relative dielectric permittivity ε_r and electrical resistivity ρ.

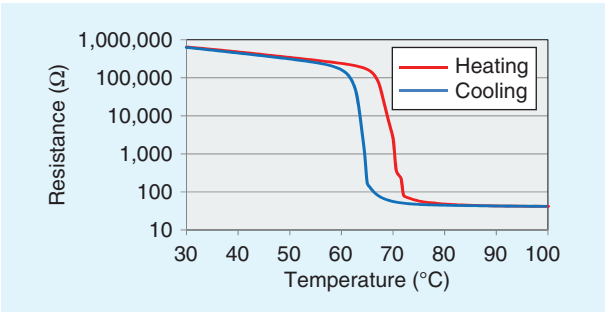

FIGURE 4. The measured dc resistance of a VO_2 film during heating and cooling.

VO_2 is a nonmagnetic material, hence, its relative magnetic permeability μ_r is one. From an engineering perspective, the IMT of the VO_2 changes its ρ and its ε_r by three to four orders of magnitude.

The abrupt changes in the properties of VO_2 make it a viable candidate for its implementation in electronic, mechanical, and optical applications. Furthermore, the fact that VO_2 is the solid–solid phase-change material with the activation temperature closest to room temperature makes it the ideal candidate for real applications where power consumption is a parameter of interest.

The hysteresis in VO_2 brings a memory capability that has been used in multiple devices for programming electrical, mechanical, and optical states [4], [25]. Thus, VO_2 is a smart multifunctional material that provides abrupt and completely reversible changes in multiple properties with a relatively low stimulus and allows for the programming of these properties.

DIELECTRIC PERMITTIVITY

Reported results demonstrate that the relative dielectric permittivity properties of the material ε_r change across the phase transition. Specifically, ε_r varies from a value near 36 at room temperature to more than 10,000 when the VO_2 is heated, as shown also in Figure 3 [26].

The shift of the dielectric permittivity value can be disregarded in simulations at the heated state due to the conduction effects overpowering the capacitive ones. It is thought that with the RF current traveling through the material during the heated state, the increase in permittivity would have little to no effect on the results.

However, in the cooled state of the VO_2, the relatively high permittivity value requires the thickness of the VO_2 and of the adjacent metal layers to be considered in the simulations. This is because there is a capacitive well created along the VO_2 patches, as explained later in the "Fabrication" section. The capacitance of the well can be found by the thickness of each substrate across the VO_2 walls that form the well. For completeness, the equivalent circuit for the VO_2 switch is illustrated in the "VO_2 for Microwave Circuits" section and is similar to others reported in series and in coplanar waveguide connections [20], [27], [28].

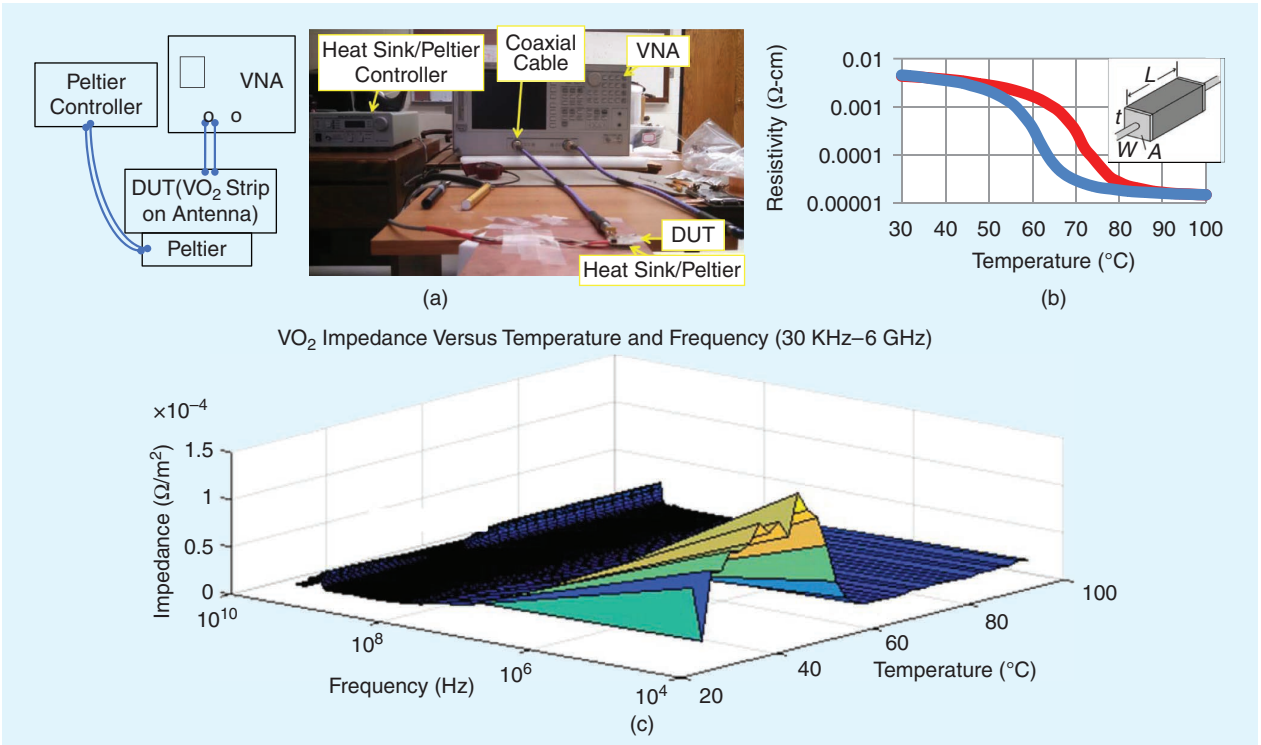

FIGURE 5. (a) The measurement setup for capturing the dc resistance changes during the thermally induced VO_2 transition. (b) The measured dc resistivity across the fabricated VO_2 during heating (red) and cooling (blue) as calculated using (1). (c) The VO_2 impedance measurement versus temperature and frequency. VNA: vector network analyzer; DUT: device under test.

RESISTIVITY

The change in VO_2 resistivity across its phase transition is largely dependent on its stoichiometry, grain size, and crystallinity. When depositing VO_2 thin films, all of these parameters are strongly dependent on the substrate. For example, VO_2 thin films grown over quartz or sapphire have larger resistivity drops across the phase transition than VO_2 thin films grown over amorphous or crystalline silicon. The extremes of this shift are dependent on what substrate the VO_2 is deposited on, and the overall variance can exceed four orders of magnitude. For comparison, copper resistivity when the temperature varies from 21 to 100 °C shifts from $1.68 \cdot 10^{-8}$ to $2.4 \cdot 10^{-8}\ \Omega \cdot \text{m}$ [29], which is negligible compared to the range of VO_2. The resistivity of resistive materials or insulators such as rubber is $1 \cdot 10^{13}\ \Omega \cdot \text{m}$.

The resistance variation of the VO_2 was measured across a 400-nm-thick polycrystalline VO_2 thin film deposited over C-cut sapphire (the same substrate structure used for the folded aperture antennas presented in the section "VO_2 for Reconfigurable Aperture Antennas—Coplanar Folded-Slot Antennas"). The resistance results are shown in Figure 4 for a full temperature cycle. A four orders-of-magnitude decrease in the resistance is observed when the VO_2 is heated.

The impedance–temperature relation of the patterned VO_2 film was also measured with respect to frequency to better understand how to use the material properties in frequency-dependent applications, such as antennas. The impedance of the VO_2 thin strip integrated on a VO_2 antenna was measured using an Agilent 8753ES S-Parameter Network Analyzer for every 2 °C from 30 to 100 °C and from 100 to 30 °C. The frequency range for these measurements was from 30 kHz to 6 GHz. The setup, shown in Figure 5(a), probed the metal adjacent to the VO_2 strip. Using the measured data, a graph for the measured impedance was made. As expected, the impedance decreased dramatically with temperature, particularly above 68 °C, featuring also a gradual decline as frequency increased. This decline is due to the thin VO_2 layer sandwiched between two thicker metallic layers that effectively create a structural well that acts as a planar-integrated capacitor. This hypothesis was validated by electromagnetic simulations where the thickness of all metal layers was considered, leading to better accuracy. The obtained data validated also the reactive behavior (energy storage and slightly reduced gain) observed on the first reported VO_2 antenna, the bowtie described in the section "VO_2 for Reconfigurable Wire Antennas—Bowtie Antennas."

VO_2 MODELING

The patches of VO_2 in this article are approximated as thin-film resistors and are modeled as such. Using method-of-moments software, such as Advanced Design System (ADS) by Keysight and IE3D by Zeland Software, a separate metal class was created and labeled as a thin-film resistor so that the material could then be directly incorporated in the antenna

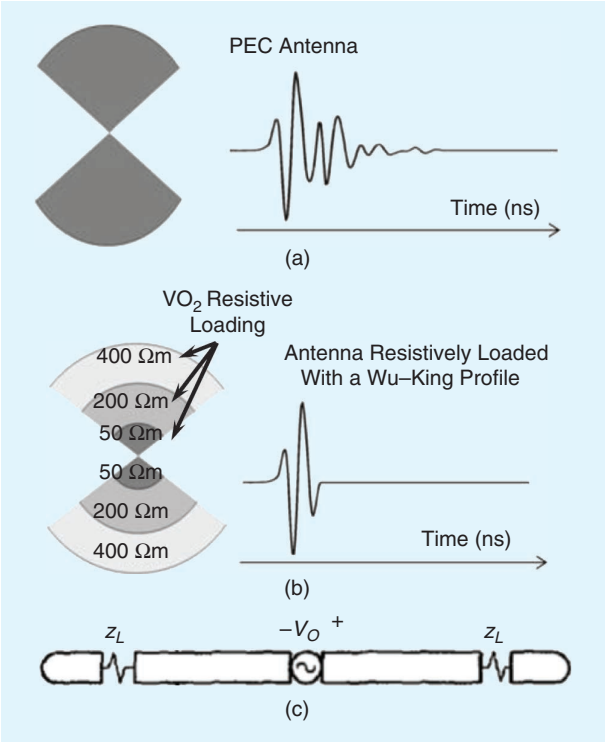

FIGURE 6. Examples of VO_2 applicability on resistively loaded antennas. (a) Metal bowties typically have increased ringing in the time domain. (b) Resistive and VO_2-loaded bowties with a Wu–King profile or wires of increasing resistance have reduced ringing and are more suitable for late-time ringing in GPRs [35]. (c) Capacitive-loaded or traveling-wave antennas [34]. PEC: perfect electric conductor.

geometry. To model each state of the VO_2, heated and cooled, the resistance material property in ohms per square (Ω/□) was altered. Measurements across square VO_2 patches determined that the values of 300 and 6 kΩ/□ are relatively accurate values for modeling the cooled and heated VO_2 states respectively for the specific fabrication technique that would be used. Due to the complex nature of VO_2, a combination of potential small variations in the thickness and stoichiometry of the material can result in large differences in patch resistance, and the material patches may not have identical electrical properties. The values were found to be sufficiently accurate, through a trial-and-error process in which fabricated wafers and antennas were measured and characterized, for use in modeling the material on a sapphire substrate.

The resistance (Ω/□) simulation values allow for the patch design process to be reduced to a simple matter of adding resistors in series and in parallel. This allows for the calculation of a specifically defined VO_2 patch. Equation (1) can be applied to find the required number of parallel squares that result in a desired resistance, in which X is the number of squares, R is the desired resistance, and R_s is the Ω/□ value:

$$\left(\frac{X}{R_s}\right)^{-1} = R. \tag{1}$$

This approach defines the width-to-length dimensions ratio required to obtain a specific resistance. For example, if 10 Ω is needed, (1) yields $X = 600$ squares. As long as the width of the material patch is 600 times larger than its length, the resistance of that patch will always be 10 Ω.

Although the measured resistance values are large, when used in an antenna structure, a parallel connection of many squares reduces the total resistance to acceptable values. Smaller resistance values have been reported in the literature [30], [31], leading to series and shunt RF switches with less than 2.2- and 0.9-dB insertion loss respectively [30], with the most common technique to reduce the resistance being the deposition of a thicker VO_2 layer. Moreover, resistive and resistively loaded antennas [e.g., antennas for ground-penetrating radars (GPRs)] that have specific profiles can take advantage of this resistance. Examples include resistive bowties, resistively loaded antennas [such as with the Wu–King profile [32], [33] in Figure 6(b) or conducting wires of increasing resistance [34] for reduced late-time ringing in GPRs [35]], and many others [36]–[45].

VO_2 FOR MICROWAVE CIRCUITS

Prototypes of microwave-frequency circuits (RF switches, RF power limiters, and phase shifters) that employ VO_2 are briefly presented next to better comprehend the VO_2 capabilities and frontiers. In [30] researchers implemented a thermally triggered VO_2 RF switch [Figure 7(b)]. In the series configuration, VO_2 acts as an open circuit below 68 °C and does not allow the RF current to pass through. When heated, VO_2 resistance drops dramatically and it allows RF current to pass through with low loss.

In [46], a power limiter was developed. It is composed of series-connected power divider/combiners with VO_2 shunts. Each resistive load, when activated, absorbs a percentage of the input power. The loads are in series to divide the transmitted power that enters in each stage of the limiter.

In [31], researchers implemented a low-loss 2-bit 50-GHz phase shifter by forming two VO_2 SP4T switches [Figure 8(b)]. The switches enable different paths of the phase shifter with electrical delay in multiples of 90°. Low losses were achieved by depositing a thicker layer of VO_2 (600 nm). The high linearity validated the use of VO_2 for wideband applications.

VO_2 FOR RECONFIGURABLE ANTENNAS

Designing a reconfigurable antenna involves altering the geometry of the structure. VO_2 has been proven capable of controlling the current flow, so two antenna prototypes, namely a planar bowtie and a folded-slot, were designed to test the effectiveness of VO_2 as a catalyst for antenna reconfigurability. The designs are based on different operating principles (bowtie as a wire antenna [47] and folded slot as an aperture) to study the application of the VO_2 on two representative classes of antennas. Also, the bowtie allows the activation of the VO_2 to result in a decrease of its resonant frequency, while the folded slot allows for it to be increased.

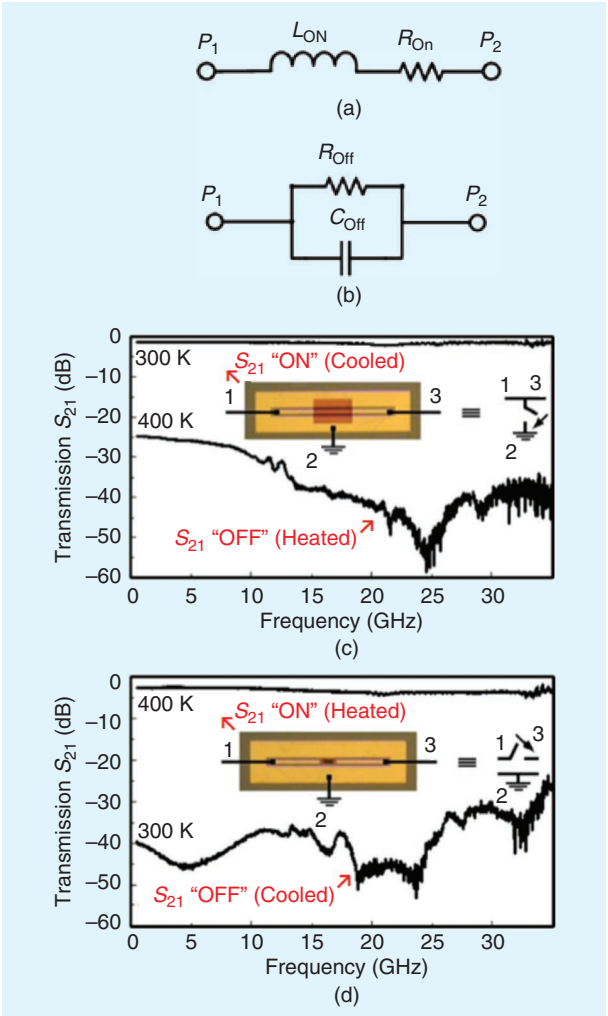

FIGURE 7. (a) The equivalent circuit of a series RF VO_2 switch in the ON state (from [20]). (b) The equivalent circuit of a series RF VO_2 switch in the OFF state (from [20]). (c) Low-loss VO_2 shunt RF switches (from [30]). (d) Low-loss VO_2 series RF switches (from [30]). (Source: Materials Research Society; used with permission.)

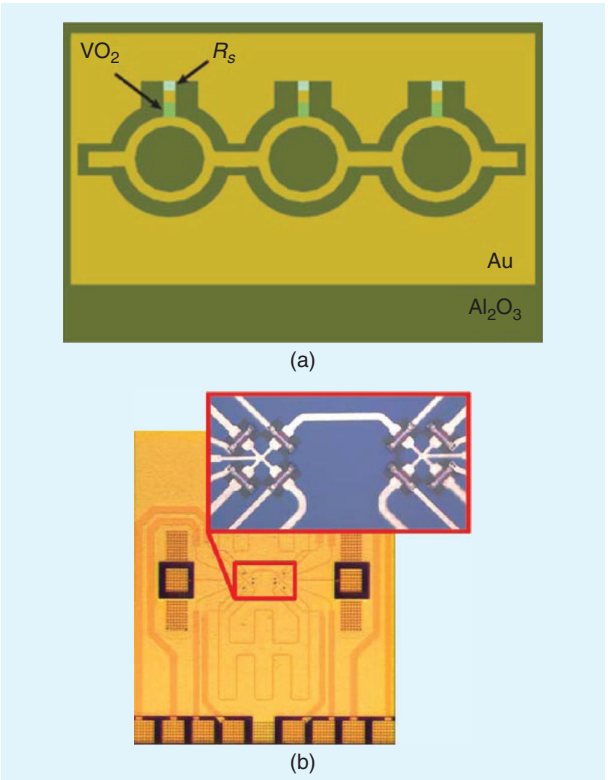

FIGURE 8. (a) A power-limiting device composed of series-connected power dividers/combiners with VO_2 shunts [46]. (b) A 50-GHz phase shifter using VO_2 with low loss (about 1 dB/bit) and high linearity [31]. Al_2O_3: aluminum oxide.

TABLE 1. DIMENSIONS FOR THE BOWTIE ANTENNA.

Dimension	L_1	L_2	H_1	H_2	W_v
Value (mm)	10.26	11.77	1.3	1.6	0.02

Each antenna was fabricated and measured, as shown later in the article. All $|S_{11}|$ measurements were taken with the antenna placed in the anechoic chamber and are compared to simulations. Pattern measurements were taken to investigate any effect of the VO_2 on the pattern shape. Additional measurements were taken to ensure that the directive heat source, required to activate the transition of the material, did not influence the data.

VO_2 FOR RECONFIGURABLE WIRE ANTENNAS—BOWTIE ANTENNAS

The first proof-of-concept antenna using VO_2 as the catalyst for reconfigurability is a bowtie design on sapphire that is fed using a coaxial sleeve balun. The VO_2 enables frequency reconfigurability by extending the length of each antenna arm symmetrically. This is achieved by depositing two 200-nm thin films of VO_2 that physically establish the connection between the two separate sections of each arm, thus enabling the two operation states. This antenna was presented in [47] and is not repeated herein. Table 1 shows the dimensions of the prototype shown in Figures 9 and 10.

The antenna was fabricated, as per the process outlined in [47], on a sapphire substrate ($\varepsilon_r = 11.5$, $\tan\delta = 0.0001$, thickness $t = 0.558$ mm), using the following steps:

1) deposition of a VO_2 thin film by pulsed-laser deposition in a 15-mTorr low-pressure chamber with controlled O_2 flow of 20 standard cm^3/min for 25 min
2) patterning by reactive ion etching (RIE) to create the two thin strips that will extend the metallization sections of the antenna
3) precise gold (AU)-layer electroplating and multiple photoresist spins.

Results indicate that the antenna indeed shifts frequency when the VO_2 undergoes a thermally induced phase change. The radiation patterns [47] were similar at both frequencies as expected. At the cooled state, the

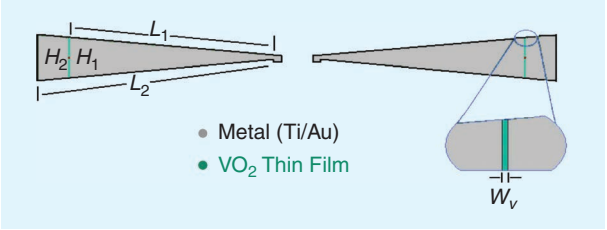

FIGURE 9. The layout of a reconfigurable bowtie antenna with VO_2 (turquoise) on both arms [47]. The VO_2 strips are only 20-μm wide. The measured gain patterns at the heated (4.58-GHz) and unheated (4.72-GHz) states showed they vary minimally, as expected for a frequency-tunable antenna.

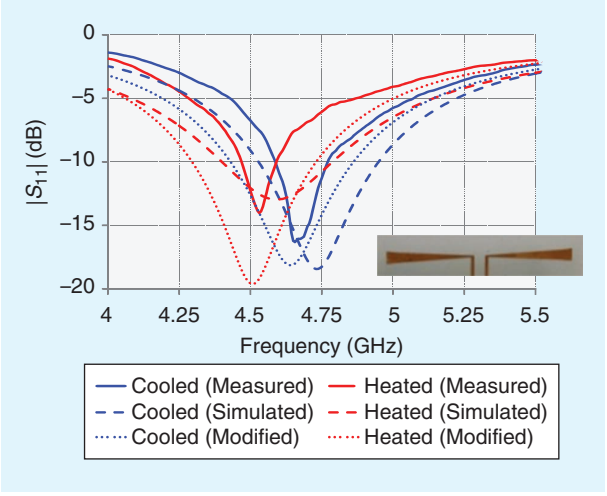

FIGURE 10. The simulated and measured $|S_{11}|$ for the heated (up to 90 °C) and cooled (to 21 °C) bowtie configurations during a hot–cold transition. The modified curves are more accurate since they use values obtained through measurements of the VO_2 impedance as described in the section "The Behavior and Physics of VO_2." The inset shows a fabricated prototype antenna with VO_2.

measured gain was 0.14 dBi with the heated state giving −0.67 dBi. As expected, the 0.8-dB gain reduction of the heated antenna was due to loss (heat) from the current passing through the VO_2, but most losses are attributed to the introduced capacitance due to the thin and narrow VO_2 film deposited adjacent to the thicker metal arms, resulting in power being stored within the antenna near field. This is due to the advantage of the VO_2 switches being extremely small (i.e., 20 μm in length). Notably, this series capacitance can be minimized by depositing a thicker and larger layer of VO_2 at the cost of having a slower switch. The thicker VO_2 will also have lower resistivity. In the future, this can enable the use of VO_2 at higher frequencies (up to several terahertz) where the metallization layers can have thickness in the order of the VO_2 layer. For the fabricated antenna, however, the calculated efficiency is 41% (heated) and 49% (cooled).

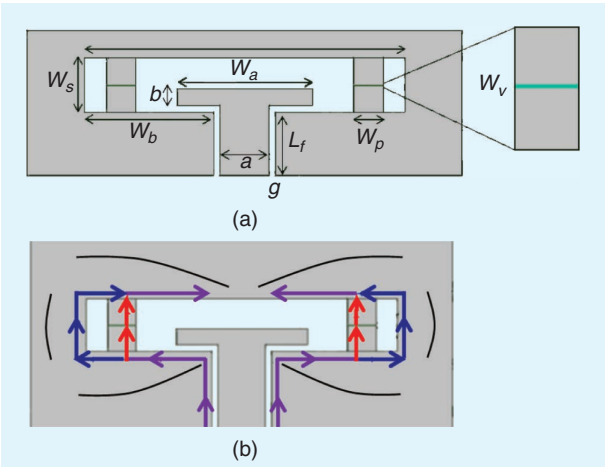

FIGURE 11. (a) The layout (not to scale) of a reconfigurable folded slot with the VO_2 (turquoise) strips on both paths reducing its circumference upon activation. (b) The operating principle of the antenna, showing the directions of the currents in each configuration (blue/red) and the standing wave of the current (black).

VO_2 FOR RECONFIGURABLE APERTURE ANTENNAS—COPLANAR FOLDED-SLOT ANTENNAS

Further investigation requires the study of a reconfigurable aperture type of antenna. It is also necessary this time to demonstrate at least 25% frequency reconfigurability. A slot or folded-slot aperture antenna allows such an investigation. In these antennas, the aperture field is created by the surrounding current. The VO_2 reduces the aperture circumference by creating short circuits on it. These short circuits increase the resonant frequency. The folded-slot design has a more stable input reactance, which allows for good matching without feed modifications, and so it was preferred.

The radiating frequency of a folded-slot aperture antenna can be defined by its parameter C, which directly relates to the perimeter of the slot defined by

$$\frac{C}{\lambda_0} = \frac{C_0}{\sqrt{\frac{(\varepsilon_r + 1)}{2}}}, \tag{2}$$

where C_0 is the value of C/λ_0 when $\varepsilon_r = 1$. Here, $C = 2 \cdot (L_s + b + W_a + W_b)$, and ε_r is the permittivity of the substrate. C_0 can be computed numerically (e.g., for $L_s/b = 0.019$, $C/\lambda_0 = 0.93$), and physically it compensates for fields outside the aperture.

Reconfigurability is enabled by adding two metallic extensions on each side of the aperture, without metallic islands (see Figure 11). Each extension pair is joined together with a narrow film of VO_2. The thin strips of VO_2 adjoin the metal pathways and elongate or shorten the perimeter and thereby decrease or increase, respectively, the frequency. The layout and operating principle of this type of antenna are shown in Figure 11.

When unheated, the VO_2 acts as an open circuit, and the current is forced to move along the perimeter of the aperture, which establishes the lower frequency of

TABLE 2. DIMENSIONS FOR THE APERTURE ANTENNA.

Dimension	W_a	W_b	W_p	W_v	W_s	L_{s_hot}	L_{s_cold}	L_{f_cold}	a	g	b
Value (mm)	6.85	6.55	1.3	0.004	2.75	11	16.2	7.5	2.5	0.3	0.85

operation. When VO_2 is heated, resistance drops to a value in which the current chooses the inner pathway establishing the higher frequency.

A major difference between the incorporation of the VO_2 in the presented prototypes is that the coplanar folded-slot antenna has a much lower resistance requirement for its heated state. To enable reconfigurability and minimize ohmic losses, the width-to-length ratio of the VO_2 film can be large. Here, the length is 4 μm with the width of 1.3 mm (total number of squares: 325), which made the VO_2 resistance 18 Ω when hot and 920 Ω when cold. The 200-nm-thick layer of VO_2 was printed on a 0.558-mm-thick aluminum oxide (Al_2O_3) substrate with $\varepsilon_r = 11.5$ and was matched to a 75-Ω transmission line (see dimensions in Table 2).

The simulated surface current confirmed the operating principle of the antenna (Figure 12). Simulated results showed a large frequency shift from 4.27 to 6.53 GHz, a shift of 52.9%, which exceeded the targeted 25%. This antenna was fabricated using the same process as that for the previous prototype. Figure 13 shows a photo of the fabricated device.

The measured $|S_{11}|$ (in Figure 14) shows a frequency shift from 4.125 to 7.1 GHz, or about 73.1%. This is equivalent to the shift achieved with MEMS that use resistive bias lines, yet the VO_2 switch is planar and more robust as it has no mechanical moving parts.

An additional comparison of the radiation patterns (Figure 15) showed good agreement as well, validating the modeling of the VO_2. The gain of the antenna in the cooled state was measured to be 1.73 dBi (calculated efficiency: 68%) with the heated state at 1.65 dBi (calculated efficiency: 64.5%). Again, the efficiency of the antenna was 4% lower at the heated state as there is again some energy stored in the capacitive well. The losses due to the VO_2 were calculated to be approximately 5.5%. To mitigate these losses, it is necessary to reduce the losses (resistance) of the heated VO_2, thus enabling longer switches with larger capacitive wells. Such low resistance values have been reported in the literature [25], [30]. The VO_2 in this prototype is very narrow (only 4-μm wide), which is arguably the shortest integrated antenna switch ever made.

In Figure 14, the cooled simulated resonance is shifted higher than the measured resonance, while the heated simulated resonance is shifted lower. In the heated state, the measured resonance was at a higher frequency than the simulated resonance due to the pin on the SMA connector feeding the antenna farther down the transmission line. Also, the wavelength is different for each frequency, so the feed does not affect all states the same. At the cooled state, the measured

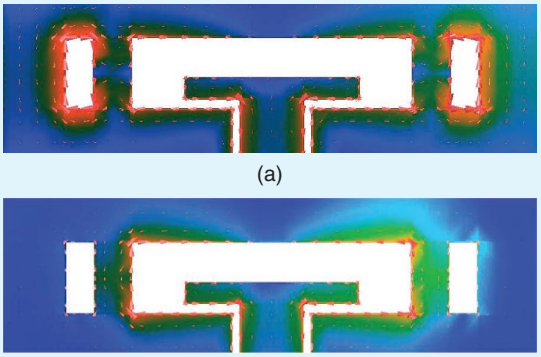

FIGURE 12. The simulated surface current flowing (a) around the full aperture when the VO_2 is unheated and (b) around the smaller aperture through the VO_2 patches when the VO_2 is heated.

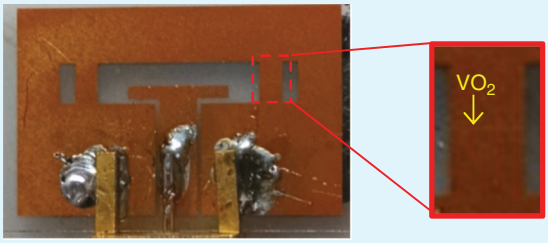

FIGURE 13. A fabricated VO_2 folded-slot antenna. The 4-μm VO_2 line appears faint and is barely visible in the inset photo.

resonance is slightly lower than the simulated resonance due to the added capacitance from the high ε_r of the VO_2, which causes current to travel farther down the inner paths before continuing around the perimeter of the slot. Further interaction with the thick SMA connector may also have affected the current path.

VO_2-INTEGRATED ANTENNA WITH RESISTIVE HEATERS

The previous two antenna prototypes validated VO_2 as a suitable material for wire and aperture types of reconfigurable antennas. The VO_2 on these antennas was activated using a convective directive heat source placed 10 cm from the antenna surface. The heater activated the transition of the material in an average of 14 s without overheating the cables. However, this heat source can be bulky and heavy. Practical commercial and defense applications often require effortless integrated actuation of the VO_2 with transition times in the range of microseconds.

To reduce the transition time, Joule heating [5] was investigated through the use of integrated resistive heaters. A video that shows the change in color of a VO_2 thin-film patch when current passes through an underlying resistive heater is available [48]. A new antenna was then designed, this time with four integrated resistive heaters, to 1) demonstrate and validate the successful integration and 2) to extract useful conclusions through the added complexity of the device having the biasing lines of the resistive heaters. Both the heaters and the bias lines are integrated within the substrate of the antenna and are not electrically connected to any part of the antenna structure, which is a major achievement in the sense as these bias lines do not interfere with the antenna.

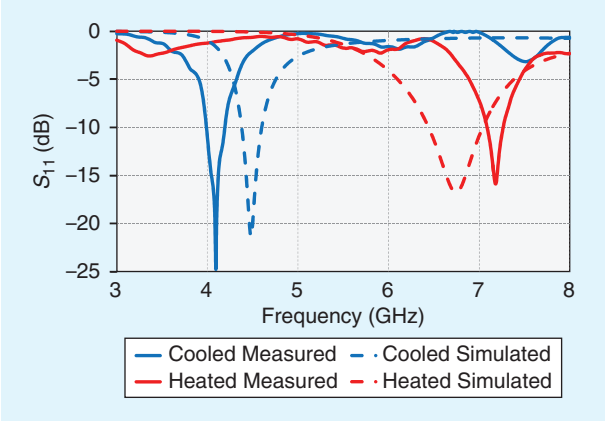

FIGURE 14. The measured and simulated $|S_{11}|$ of the VO_2 folded-slot antenna.

DESIGN

The antenna design that was used is a coplanar folded-slot antenna with a smaller aperture to address X-band applications. This design incorporates four VO_2 thin-film patches placed at the edges of each metal strip, as shown in Figure 16. Under each VO_2 film is a silicon dioxide (SiO_2) isolation layer, and under that layer a platinum (Pt)-resistive heater is deposited along with the dc bias lines that extend underneath the antenna, as shown in Figure 17. As the dc lines pass largely underneath the ground layer of the antenna, while most fields are concentrated in the aperture area, the interference of the lines with the antenna impedance and pattern's shape is negligible. All dimensions are in Table 3. Simulated results for the antenna showed that frequency reconfigurability is achieved with the two resonant frequencies being at 9 GHz (cold VO_2) and 11 GHz (hot VO_2).

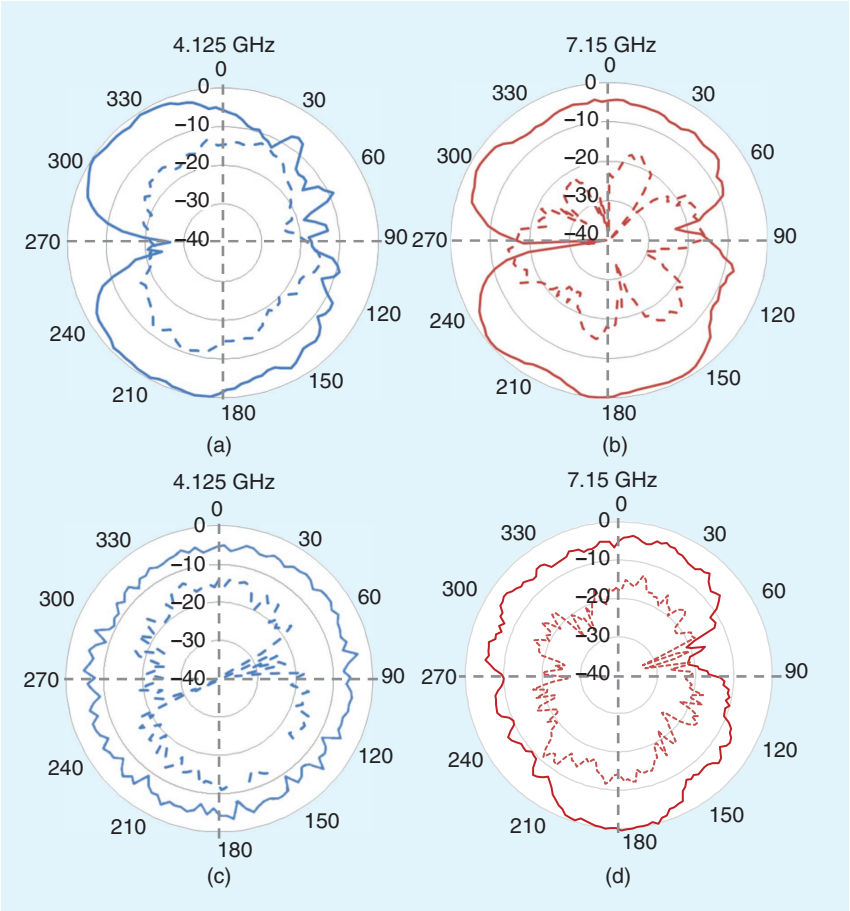

FIGURE 15. The measured radiation patterns of the VO_2 folded-slot antenna. Solid lines: copolarization; dashed lines: cross polarization. (a) E-plane, unheated. (b) E-plane, heated. (c) H-plane, unheated. (d) H-plane, heated.

FABRICATION

The fabrication process for the antennas with dc bias (see Figure 18) started with the deposition and patterning of resistive heaters and insulating SiO_2 film. A sapphire (Al_2O_3) wafer (5.08 cm in diameter and 558-μm thick) was used as a starting substrate. The resistive heaters and dc bias lines were defined by using standard metal liftoff of a Ti/Pt layer (50/150 nm). It is necessary to use a high-temperature metal (e.g., Pt) for the dc bias lines and resistive heater, since the deposition of VO_2 occurs at approximately 470 °C. After the dc bias and resistive heaters have been defined, a layer of SiO_2 (1 μm) was deposited over the entire surface. This layer is necessary to electrically isolate the VO_2 film (next film deposition) from the resistive lines. After the deposition of the dc bias lines, resistive heaters, and insulating SiO_2 layer, the steps of the fabrication process for both types of antennas was very similar. The next step in the process is the deposition of the VO_2 thin film.

VO_2 PATTERNING AND ANTENNA METALLIZATION

VO_2 patterning was done using RIE, which is a dry etching technique. The etching parameters and conditions are similar to those reported in [46] and [49]. This technique has resulted in well-defined VO_2 patches with smooth side walls for feature sizes as small as 4 μm. After the VO_2 patches are defined, openings in the SiO_2 layer over the metal pads that connect to the resistive heaters were defined using RIE as well [see Figure 18(d), inset]. Next in the fabrication process, the patterned VO_2 patches were covered with photoresist, and a Ti/Au seeding layer (40/160 nm) was deposited over the substrate. The continuity of the Ti/Au layer was verified by measuring resistance at different points on the substrate. The photoresist layer that covered the patterned VO_2 patches is removed after the seeding layer is deposited. Next, photoresist (2.3-μm thick) was spun and patterned, leaving only the antenna metallization exposed in the area defined by the antenna design; i.e., the photoresist is used as a soft mask. The outer border of the surface of the wafer was cleaned manually with acetone, removing a ring of ~ 2 μm- of photoresist over the substrate surface. The Au layer exposed in this ring will be in contact with the electroplating sample holder. During the first 2.3 μm of Au growth, the pattern is well defined by the walls of the photoresist; but after this, the metallization grows isotropically and does not follow exactly the pattern defined on the photoresist. Given the thin VO_2 patches that separate the antenna metallization, the design and processing time had to consider side growth of the Au because, after growing thicker than the 2.3 μm of the photoresist wall, the antenna could grow over the VO_2 and create a short circuit with its extension.

After electroplating, the photoresist mask is removed and a thickness of the antenna metallization of ~ 4.15 μm was measured using a profilometer. The Au seeding layer (which did not grow during electroplating since it was covered with the photoresist mask) was removed with a quick dip in Au etchant (potassium iodide). The VO_2 strips were exposed during the removing of the seeding Au layer, but it was verified in previous experiments that VO_2 thin films are not attacked by Au etchant solutions. However, the removal of the Ti-seeding layer involved wet etching, and the VO_2 strips needed to be protected from this step. Thus, before removing the Ti-seeding layer through buffered oxide etching, an adhesion promoter (hexamethyldisilizane) was spun on the sample, followed by a photoresist layer that was patterned to protect the VO_2. In the final step, the photoresist layer is removed.

The result of this integration procedure is a resistive heater just underneath each strip of VO_2. The resistive heaters were tested at dc with a regulated current source. A photo of the fabricated prototype is shown in Figure 19. The dc pads and the SMA connector are also visible for scaling.

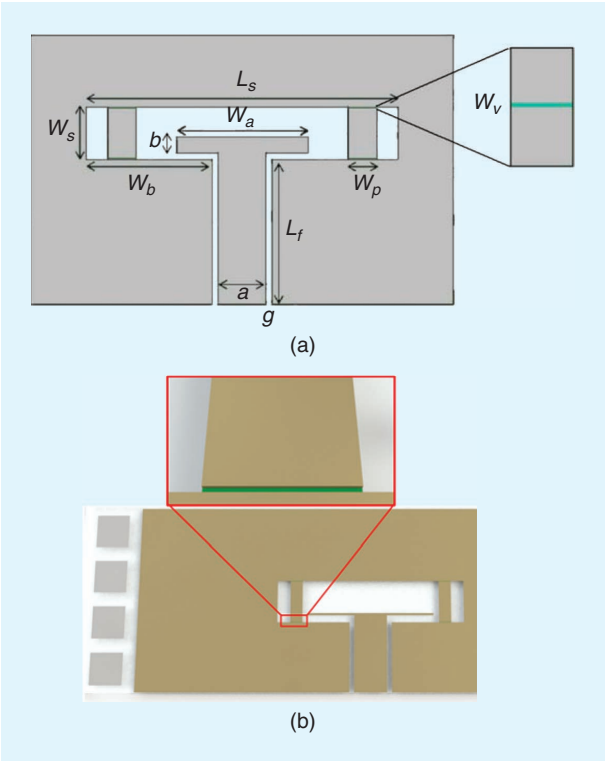

FIGURE 16. A folded aperture antenna with four VO_2 thin-film strips. (a) The 2D plot, top view. (b) The 3D plot showing the VO_2 and metallization layers in scale.

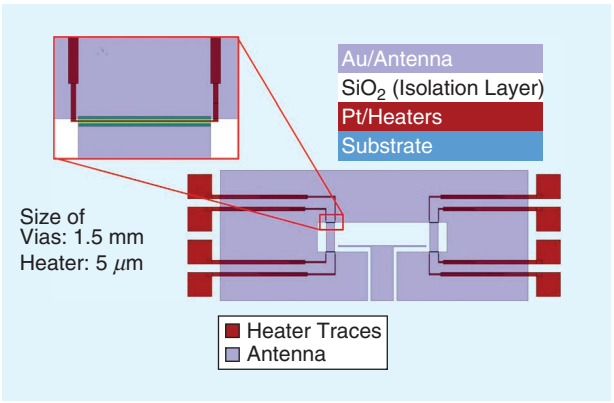

FIGURE 17. The integration of four VO_2 thin-film strips with resistive heaters and bias lines (red) that are monolithically etched underneath the antenna layer (purple). The inset shows the detail of the resistive heater and VO_2 on the layout. The aperture area covered by the dc lines is negligible.

TABLE 3. DIMENSIONS FOR THE ANTENNA WITH INTEGRATED HEATERS.

Dimension	W_a	W_b	W_p	W_v	W_s	L_{s_hot}	L_{s_cold}	L_{f_cold}	a	g	b
Value (mm)	5.4	3.1	5.25	0.02	1.8	6.35	8	3	1.4	0.2	0.1

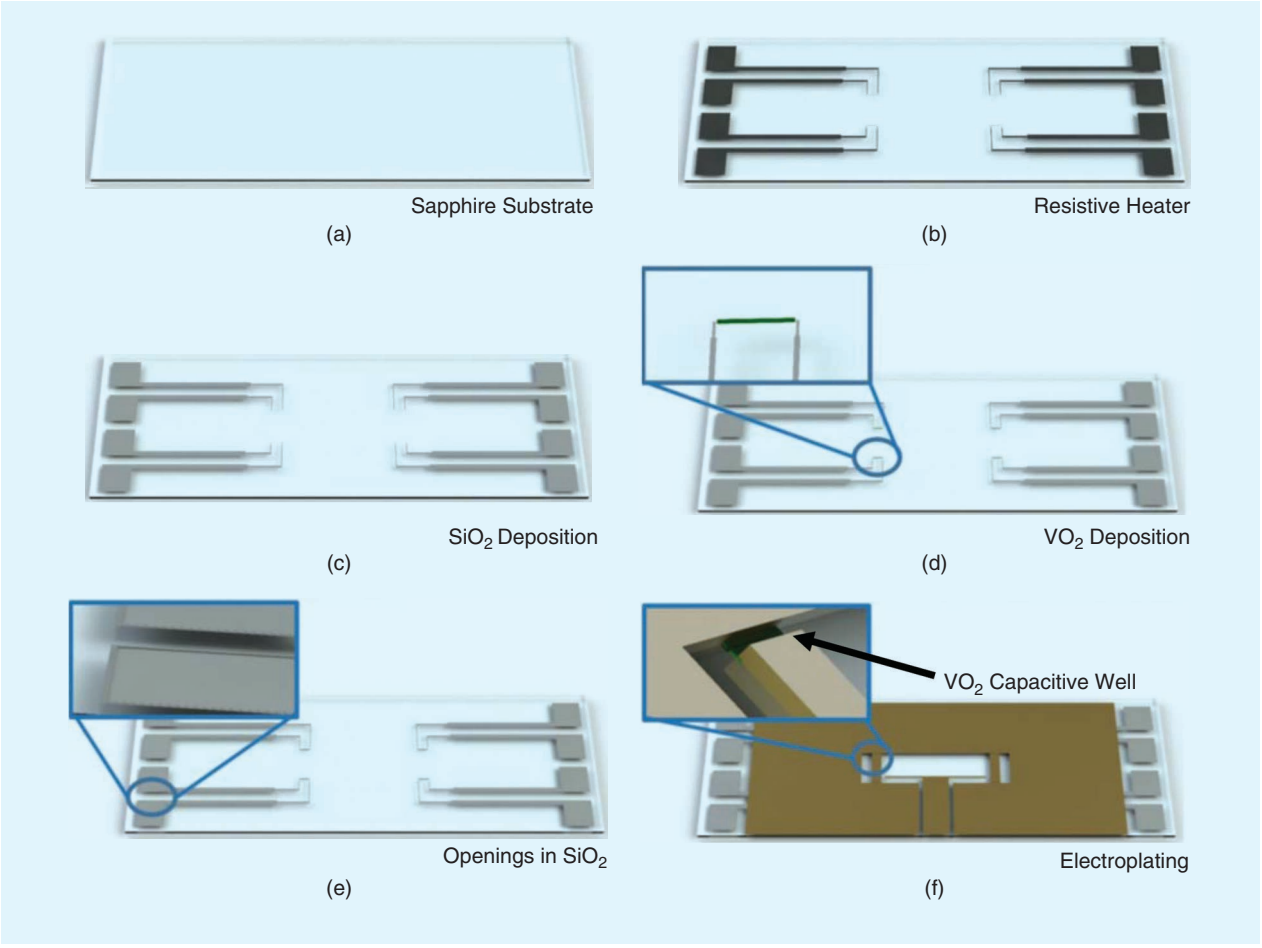

FIGURE 18. The summarized fabrication process flow of the VO_2 antennas with heaters. (a) The starting substrate: sapphire substrate (C cut). (b) The deposition of Ti/Pt metal electrodes for resistive heaters and wire-bonding contact pads. (c) The deposition (by plasma enhanced chemical vapor deposition) and patterning (by RIE) of the thin SiO_2 layer. (d) The deposition (by pulsed laser) and patterning (by RIE) of VO_2. (e) The etching of the SiO_2 layer over wire-bonding pads that connect to resistive heaters. (f) The electroplating of Au.

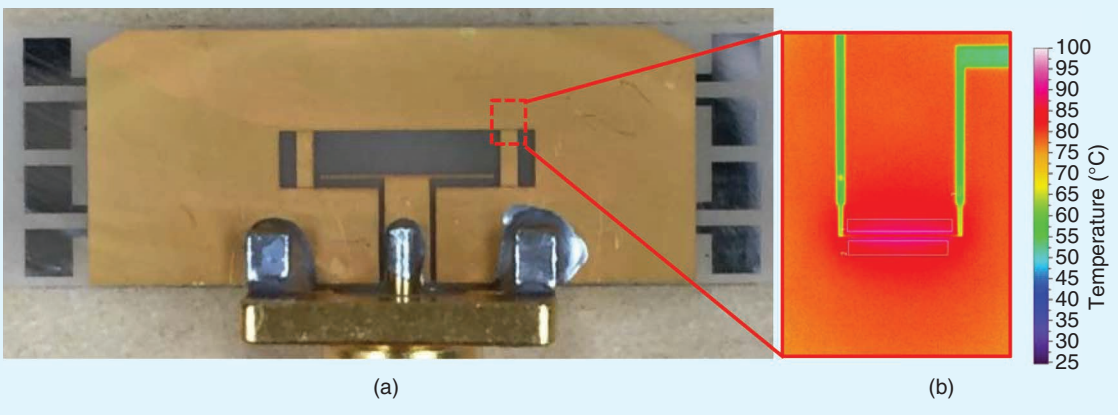

FIGURE 19. (a) A fabricated antenna prototype with integrated resistive heaters. The dc pads and lines pass underneath the antenna metallization layer and are isolated by thin SiO_2. Then, they are moved to the top layer with vias. The inset (b) encircles a VO_2 strip. The measured heat distribution on the heater at actuation is also shown.

As mentioned previously, the short discontinuities of the metal layers, which are filled with VO_2 of relatively high permittivity value, require the thickness of the VO_2 and adjacent metal layers to be considered in the simulations. This is because there is a capacitive well created along the VO_2 patches due to coupling between the disconnected metal edges of the device, which are a few microns tall. The thin (tenths of a micrometer) VO_2 layer is sitting at the bottom of

this well [see Figure 18(f)]. This capacitive well can also be observed in Figure 16(b).

MEASUREMENT RESULTS

The measurement setup consists of a Keithley 2400 Sourcemeter used as a regulated voltage and current source. The VO_2 transition occurred after 40 μs at a temperature of 90 °C by supplying 84-mA dc current at 20.7 V. The total power consumption was 1.74 W. Figure 19 shows also the measured heat distribution on the resistive heater at actuation. The image was taken using the OptoTherm Micro System thermal microscope and the Thermalyze thermal image analysis software from Optotherm Thermal Imaging.

Figure 20 shows the measured $|S_{11}|$. The resonance shifted from 9 GHz (cooled) to 11–13 GHz (heated), indicating a 33% increase. Simulated results indicate that the VO_2 modeling and the implementation of the design were successful.

VO_2 ANTENNA RADOMES AND CLOAKING

The metal–insulator transition of the VO_2 can find additional applications as an antenna radiation cloak or reconfigurable radome. For example, an entire sheet of transparent (insulating) VO_2 will let microwave radiation pass through it, while when heated its RF-absorbing (conductive but resistive) state will prevent radiation from passing through. When there is no need to transmit or receive, the antenna can be cloaked rapidly behind the RF-absorbing material.

An experimental investigation of the properties of VO_2 in a cloaking application was conducted next. Two Flann Microwave DP240 2–18-GHz directive horns facing each other were placed at a 2-m distance. A 2 in (5.08 cm) in diameter Al_2O_3 wafer with 200-nm-thick VO_2 deposited on it (Figure 21) was placed directly in front of one of the horns, which had an opening of 13.5 cm in diameter. The transmission between the two antennas was then measured by means of the S_{21} parameter, removing the free-space path loss.

The VO_2 wafer was heated convectively and results were compared with the free-space scenario and with a full-metal (copper) wafer. At room temperature, the VO_2 wafer acted as a dielectric with some diffraction effects adding to the overall signal transmission compared to the attenuation of free space (i.e., without the wafer), as shown in Figure 21. When heated, the VO_2 reduced the $|S_{21}|$ by about 4.5 dB, which is an attenuation comparable to that of a 1-in copper disk. This reduction to the transmitted signal indicates that VO_2 can be used to hide antennas and reveal them on demand, to block or allow reception of signals respectively.

The circular VO_2 "rainbows" in the 2-in wafer in Figure 21 are due to the variation in the VO_2 thickness and stoichiometry across the wafer, which varies with deposition temperature (the temperature on the wafer during deposition decreases radially from the center). Nevertheless, this change in stoichiometry is not large enough to cause a low-quality film.

DISCUSSION

A phase-change material (VO_2) was demonstrated to be a suitable material for use in reconfigurable antenna designs. We presented proof-of-concept reconfigurable prototypes

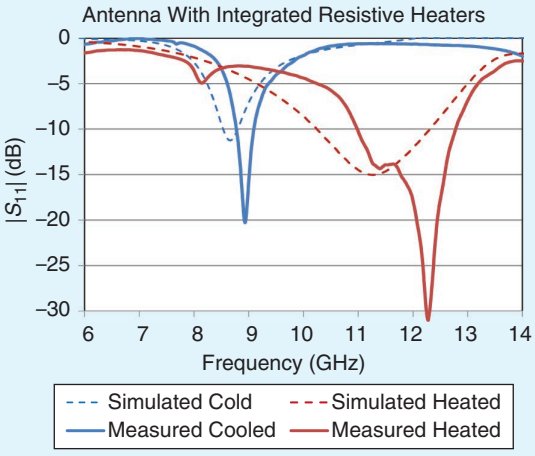

FIGURE 20. The measured and simulated $|S_{11}|$ of the VO_2 antenna with integrated resistive heaters, demonstrating a large frequency shift when the VO_2 is heated.

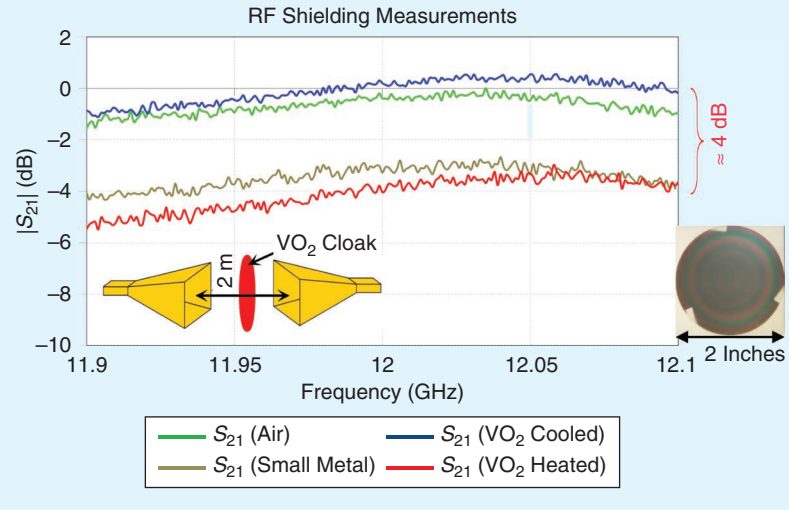

FIGURE 21. The measured results from the investigation of VO_2 as an antenna shield on demand. Results indicate a 4-dB attenuation of the transmission coefficient when the VO_2 test wafer is heated compared to the cooled VO_2, which exhibits a transmission coefficient similar to that of air with the added contributions from diffraction that enhance the signal. Inset: the fabricated test wafer with 200-nm-thick VO_2 used for proof-of-concept cloaking measurements.

for wire and aperture antennas and novel designs and methodologies, including the bandwidth reconfigurable antenna, the antenna with integrated resistive heaters, and the reconfigurable cloak. It was shown that VO_2 performs reasonably as a catalyst for reconfigurability when its phase change is thermally induced.

TECHNOLOGY COMPARISON

Table 4 includes a comparison of the presented VO_2 switch technology to semiconducting and MEMS switches. The comparison is based on published measured results and specification sheets available in the literature. Though not comprehensive, the comparison can serve as a reference for the feasible performance and device design space.

Advantages of using integrated heaters for the VO_2 include ease of actuation, minimal coupling from the biasing circuit for higher accuracy, and precise temperature control to record and program the different states of an antenna. Moreover, the VO_2 switch is arguably one of the smallest (shortest in length) used in a reconfigurable antenna structure. The extremely small area of the VO_2 necessary in some of the presented antennas (a few micrometers, e.g., 20-μm width by 200-nm height) allows for the heating to take place using low power. Also, the RF linearity reported for this material is excellent, as it does not rely on semiconducting components. Rather, it relies on the rearrangement of the electrons in the material lattice.

TABLE 4. A COMPARISON OF SOME EXISTING SWITCHING TECHNOLOGIES WITH THE PROPOSED VO_2 TECHNOLOGY.

	p-i-n Diodes and FET Transistors*	MEMS Switches†	Proposed VO_2 Switches Technology
Reliability	Excellent	Millions to billions cycles	Trillions of cycles‡ (estimated)
Durability/robustness	Average (soldering)	Average (soldering)	Excellent (flush mounted; no solder) [1]
Linearity/intermodulation distortion	Nonlinear for large bandwidths	Excellent	Excellent (estimated; best reported)
Actuation	0.7 V, 1 mA; (FET: 0.3–0.4 V)	~15–40 V	Thermal (68 °C), optical, laser, infrared
Highest frequency	<40 GHz	~40 GHz	>10 THz¶ estimated; not yet demonstrated
Switching time	ns	1–300 ms	2 ns–40 μs (size dependent) [23]
Fabrication yield	High	Medium	High (estimated; under development)
Tuning bandwidth limited	Yes, due to biasing circuit	Yes, due to biasing circuit	No limit (thanks to remote actuation)
High-resistive lines	Not applicable	Required in some designs	Not required
Power to switch	1 mW (approximately)	As low as ~0.1 mW	1–1,000 mW (size dependent)
Packaging	Required/commercial off the shelf	Required	Not required‡
Hot switching	Yes (diodes); No (FET)	No	Yes
Size	~2 × 2 mm	~150 × 350 μm	~20 × 20 μm^2 to 1,000 × 1,000 μm^2, varies
Shunt configuration	IL_{ON} < 0.2 dB @ 0.5 GHz, 1.2 dB @ 5 GHz ISO_{OFF} ≈ 30 to 1 dB	IL_{ON} ~ 0.6 dB ISO_{OFF} > 20 dB	IL_{ON} < 0.3 dB (estimate) ISO_{OFF} > 25 dB
Series configuration	IL_{ON} < 0.1 dB @ 0.5 GHz, >5 dB @ 5 GHz ISO_{OFF} ≈ 40 to 3 dB	IL_{ON} < 0.3 dB ISO_{OFF} < −15 dB	IL_{ON} < 1 dB (reducible) ISO_{OFF} < −20 dB

IL: insertion loss; ISO: isolation.

*Specifications from Avago Technologies; Hewlett-Packard "Application Note 922" (www.qsl.net/n9zia/wireless/pdf/an922.pdf); C.-L. Lim, "Designing an PIN diode switch for high-linearity applications, *EE Times* (http://www.eetimes.com/document.asp?doc_id=1276365).

†Specifications from Radant MEMS Specifications (https://web.archive.org/web/20170313092854/http://radantmems.com/radantmems/switchperformance.html).

‡As long as the VO_2 is not operated in extremely harsh environments (e.g., above 250 °C, in an oxidizing atmosphere, or in any acidic or basic solutions), it should sustain that many actuation cycles.

¶As long as the VO_2 is not taken to extreme environments.

ACTUATION MECHANISM

The variety of methods to induce this phase change (thermal via conductive heating, thermal via Joule heating, photothermal, voltage difference, remote optical excitation via laser) eliminates the need for wired biasing. Because the actuation mechanism of the VO_2 is decoupled from the antenna, the antenna engineer has an additional degree of freedom, permitting reconfigurability without the limitations imposed by traditional electrically connected biasing circuits. This enables large structures, such as reconfigurable arrays and reflectarrays with hundreds of elements, to be realized. The remote actuation capability of VO_2 (e.g., through the heat of a laser) further removes completely the need for any form of biasing network and enables new designs that are optically activated, dynamically reconfigurable, and able to be actuated extremely fast for real-time communication, surveillance, sensing, and security applications.

FABRICATION

The complexity of fabrication may impose limitations on the substrates used. However, fabrication should be simpler than for MEMS as it does not involve suspended cantilever photolithography [13], [50]. Cost will highly depend on the substrate (e.g., sapphire or quartz). For the switches in this article, at the time of writing, cost was estimated at US$0.2 to US$0.5 per mm^2 with a time to fabrication of one day in a research laboratory, allowing designs with resolution down to 4 μm or lower.

TRANSITION TIME LIMIT

The implementation of integrated resistive heaters on wafer allows for faster and seamless electronic actuation of the VO_2. Reconfiguration speed for RF applications is approximately 10 μs, which is on a par with MEMS. Transition time, however, relates to the volume of the VO_2 that needs to be heated. Transitions with rise times as fast as 2 ns have been reported [51] when the VO_2 was grown directly on the tips of metal electrodes spaced a few hundreds of nanometers apart. The Joule heating is expected to facilitate fast actuation speeds as long as the area of the VO_2 remains relatively small.

PACKAGING

VO_2 does not require packaging in nonextreme environments. Also, the hysteresis of the transition allows for small temperature fluctuations without affecting device performance. All measurements were taken in a controlled laboratory environment with relatively stable temperature, and there was no need for packaging. Also, the switch was robust to human touch. The system can be sensitive to random large temperature fluctuations in the environment, especially during the phase-transition region. Technically, if we want the VO_2 to be robust against changes of temperature in the environment, then we need to either include a control system to the circuitry used to actuate the VO_2 or some form of packaging. With rapid heating, cooling, and feedback mechanisms, the device temperature could be stabilized even in fluctuating temperature conditions and be made suitable for outdoor terrestrial and space environments (e.g., satellite antennas or mobile phone base stations).

ROBUSTNESS

The fabricated integrated prototypes are very robust, and device lifetime is expected to be very long since no moving parts or soldering is required. Weight and size are estimated to be the smallest among all existing technologies (p-i-n diodes, varactors, FET transistors, and MEMS), most of which come in a package. The low transition temperature (68 °C) ensures no damage or significant expansion due to the conduction of heat to nearby cables and circuits. Convective heating even up to 80 °C conforms to all standard coaxial cables (e.g., RG-58, RG-59 [52], [53]), military cables (they are rated up to 105 °C [54]), SMA connectors (rated to 165 °C [55]), Polytetrafluoroethylene Teflon insulation of coaxial cables (rated to 160 °C [56]), most common dielectrics, paper, and off-the-shelf components, such as p-i-n diodes (rated to 125 °C) [57]. Moreover, localized Joule heating does not propagate to damage other parts of the antenna and add noise directly into the receiver.

POWER CONSUMPTION

On the other hand, power consumption is higher than it is for most other technologies, with a 1–2-W (20 V, 80 mA) estimated requirement for actuation, mainly due to the high current needed to increase the temperature of the VO_2.

CONCLUSIONS

The fabrication and integration challenges of VO_2 with a focus on reconfigurable antennas and microwave devices were presented. Results clearly demonstrate that VO_2 can be used for more than RF switches, while there is space and need for improvements. There are multiple dimensions in this tradeoff space of reconfigurable components using VO_2. VO_2 is a promising material that enables new components, new designs, and new fundamental building blocks in RF design. Further research for loss reduction and accurate resistivity control can make this a very promising material for wideband RF applications and can lead to new designs that fully use the unique capabilities of the VO_2-integrated thin-film switches that may replace other off-the-shelf components. In addition, the implications of the measured hysteresis curve can be explored to enable programmable devices and lead to other exciting discoveries. This article is supported by online multimedia material in IEEE DataPort [48].

ACKNOWLEDGMENTS

This work was supported by the National Science Foundation, under grants ECS-1310400 and ECS-1310257, and by the EU H2020 Marie Skłodowska-Curie Individual Fellowship ViSionRF grant 840854. We thank Brenden Dixon and Nathan Kovarik for assisting with the antenna measurements.

AUTHOR INFORMATION

Dimitris E. Anagnostou (d.anagnostou@hw.ac.uk) is an associate professor with the Institute of Sensors, Signals, and Systems

at Heriot-Watt University, Edinburgh, United Kingdom. His research interests include reconfigurable antennas, arrays, and radio-frequency front ends, functional materials, radar, and wireless sensing for health care, 5G, metasurfaces, and microelectromechanical systems. He is currently a Marie Curie fellow and a Senior Member of the IEEE.

David Torres (David.torres-reyes.1@us.af.mil) is an electronic engineer with the U.S. Air Force Research Laboratories, Wright-Patterson Air Force Base, Ohio. His research interests include functional materials. He received his B.S. degree in electrical engineering from the University of Puerto Rico, Mayagüez, and his Ph.D. degree in electrical engineering from Michigan State University, East Lansing.

Tarron S. Teeslink (tarron.teeslink@outlook.com) is a senior engineer with Echodyne, Kirkland, Washington. His research interests include reconfigurable antennas.

Nelson Sepulveda (sepulve6@msu.edu) is an associate professor with the Electrical and Computer Engineering Department, Michigan State University, East Lansing. His current research is focused on smart materials and their integration in multifunctional devices, flexible piezoelectric/ferroelectret devices, and electromechanical energy-harvesting systems. He is a Senior Member of the IEEE.

REFERENCES

[1] F. Morin, "Oxides which show a metal-to-insulator transition at the Néel temperature," *Phys. Rev. Lett.*, vol. 3, p. 34, July 1959. doi: 10.1103/PhysRevLett.3.34.

[2] K. J. Kaltenecker, J. Leroy, A. Crunteanu, G. Humbert, B. M. Fischer, and M. Walther, "THz metamaterials based on metal–insulator transition of VO_2 patterns," in *Proc. 39th Int. Conf. Infrared, Millimeter, and Terahertz Waves*, 2014., pp. 1–2. doi: 10.1109/IRMMW-THz.2014.6956210.

[3] P. U. Jepsen et al., "Metal-insulator phase transition in a VO_2 thin film observed with terahertz spectroscopy," *Phys. Rev. B*, vol. 74, no. 20, p. 205,103, Nov. 2006. doi: 10.1103/PhysRevB.74.205103.

[4] H. Coy, R. Cabrera, N. Sepúlveda, and F. E. Fernández, "Opto-electronic and full-optical multiple state memory response in phase-change materials," *J Appl. Phys.*, vol. 108, no. 11, p. 113,115, 2010. doi: 10.1063/1.3518508.

[5] R. Cabrera, E. Merced, and N. Sepúlveda, "Performance of electro-thermally driven VO_2-based MEMS actuators," *J. Microelectromech. Syst.*, vol. 23, no. 1, pp. 243–251, 2014. doi: 10.1109/JMEMS.2013.2271774.

[6] E. Merced, N. Dávila, D. Torres, R. Cabrera, F. E. Fernández, and N. Sepúlveda, "Photothermal actuation of VO_2:Cr-coated micro-cantilevers in air and aqueous media," *Smart Mater. Struct.*, vol. 21, no. 10, p. 105,009, Aug. 2012. doi: 10.1088/0964-1726/21/10/105009.

[7] B. Wu, A. Zimmers, H. Aubin, R. Ghosh, Y. Liu, and R. Lopez, "Electric-field-driven phase transition in vanadium dioxide," *Phys. Rev. B*, vol. 84, p. 241410(R), Dec. 2011. doi: 10.1103/PhysRevB.84.241410.

[8] A. Cavalleri et al., "Femtosecond structural dynamics in VO_2 during an ultrafast solid-solid phase transition," *Phys. Rev. Lett.*, vol. 87, no. 23, p. 237,401, 2001. doi: 10.1103/PhysRevLett.87.237401.

[9] G. H. Huff and J. T. Bernhard, "Integration of packaged RF MEMS switches with radiation pattern reconfigurable square spiral microstrip antennas," *IEEE Trans. Antennas Propag.*, vol. 54, no. 2, pp. 464–469, 2006. doi: 10.1109/TAP.2005.863409.

[10] G. M. Rebeiz et al., "Tuning in to RF MEMS," *IEEE Microw. Mag.*, vol. 10, no. 6, pp. 55–72, 2009. doi: 10.1109/MMM.2009.933592.

[11] D. E. Anagnostou et al., "Design, fabrication, and measurements of an RF-MEMS-based self-similar reconfigurable antenna," *IEEE Trans. Antennas Propag.*, vol. 54, no. 2, pp. 422–432, 2006. doi: 10.1109/TAP.2005.863399.

[12] Y. Huang, A. Sai Sarathi Vasan, R. Doraiswami, M. Osterman, and M. Pecht, "MEMS reliability review," *IEEE Trans. Device Mater. Rel.*, vol. 12, no. 2, pp. 482–493, June 2012. doi: 10.1109/TDMR.2012.2191291.

[13] D. A. Czaplewski, C. D. Nordquist, G. A. Patrizi, G. M. Kraus, and W. D. Cowan, "RF MEMS switches with RuO2–Au contacts cycled to 10 billion cycles," *J. Microelectromech. Syst.*, vol. 22, no. 3, pp. 655–661, June 2013. doi: 10.1109/JMEMS.2013.2239256.

[14] D. Peroulis, K. Sarabandi, and L. P. B. Katehi, "Design of reconfigurable slot antennas," *IEEE Trans. Antennas Propag.*, vol. 53, no. 2, pp. 645–654, Feb. 2005. doi: 10.1109/TAP.2004.841339.

[15] P. Bhartia and I. J. Bahl, "Frequency agile microstrip antennas," *Microw. J.*, vol. 25, pp. 67–70, Oct. 1982.

[16] S. Kawasaki and T. Itoh, "A slot antenna with electronically tunable length," in *Proc. IEEE APS Int. Symp.*, vol. 1. London, ON: IEEE, 1991, pp. 130–133. doi: 10.1109/APS.1991.174790.

[17] D. J. Chung, D. E. Anagnostou, G. Ponchak, M. Tentzeris, and J. Papapolymerou, "Integration of a 4×8 antenna array with a reconfigurable 2-bit phase shifter using RF-MEMS switches on multilayer organic substrates," in *Proc. IEEE APS/URSI Int. Symp.*, Honolulu, HI, June 10–15, 2007, pp. 93–96. doi: 10.1109/APS.2007.4395438.

[18] N. Kingsley and J. Papapolymerou, "Organic 'wafer-scale' packaged miniature 4-bit RF MEMS phase shifter," *IEEE Trans Microw. Theory Techn.*, vol. 54, no. 3, pp. 1229–1236, Mar. 2006. doi: 10.1109/TMTT.2005.864099.

[19] C. Lugo and J. Papapolymerou, "Six-state reconfigurable filter structure for antenna based systems," *IEEE Trans. Antennas Propag.*, vol. 54, no. 2, pp. 479–483, Feb. 2006. doi: 10.1109/TAP.2005.863386.

[20] J. Lee et al., "Epitaxial VO_2 thin film-based radio-frequency switches with thermal activation," *Appl. Phys. Lett.*, vol. 111, no. 6, p. 063110, July 2017. doi: 10.1063/1.4998452.

[21] S. Yang, M. Vaseem, and A. Shamim, "Fully inkjet-printed VO_2-based radio-frequency switches for flexible reconfigurable components," *Adv. Mater.*, vol. 4, no. 1, p. 180,0276, Jan. 2019. doi: 10.1002/admt.201800276.

[22] U. Chettial and N. Enghetta, "Modeling vanadium dioxide phase transition due to continuous-wave optical signals," *Optics Exp.*, vol. 23, no. 1, pp. 445–451, 2015. doi: 10.1364/OE.23.000445.

[23] S. D. Ha, Y. Zhou, A. E. Duwel, D. W. White, and S. Ramanathan, "Quick switch: Strongly correlated electronic phase transition systems for cutting-edge microwave devices," *IEEE Microw. Mag.*, vol. 15, no. 6, pp. 32–44, Sept.–Oct. 2014. doi: 10.1109/MMM.2014.2332422.

[24] J. D. Budai et al., "Metallization of vanadium dioxide driven by large phonon entropy," *Nature*, vol. 515, no. 7528, pp. 535–539, 2014. doi: 10.1038/nature13865.

[25] R. Cabrera, E. Merced, and N. Sepúlveda, "A micro-electro-mechanical memory based on the structural phase transition of VO_2," *Phys. Status Solidi A*, vol. 210, pp. 1704–1711, Aug. 2013. doi: 10.1002/pssa.201330021.

[26] Z. Yang, C. Ko, V. Balakrishnan, G. Gopalakrishnan, and S. Ramanathan, "Dielectric and carrier transport properties of vanadium dioxide thin films across the phase transition utilizing gated capacitor devices," *Phys. Rev. B*, vol. 82, no. 20, p. 205,101, Nov. 1, 2010. doi: 10.1103/PhysRevB.82.205101.

[27] N. Shukla et al., "Synchronized charge oscillations in correlated electron systems," *Sci. Rep.*, vol. 4, no. 1, art. no. 4964, May 2014. doi: 10.1038/srep04964.

[28] S. Ha, Y. Zhou, C. Fisher, S. Ramanathan, and J. Treadway, "Electrical switching dynamics and broadband microwave characteristics of VO_2 radio frequency devices," *J Appl. Phys.*, vol. 113, no. 18, p. 184,501, 2013. doi: 10.1063/1.4803688.

[29] R. A. Matula, "Electrical resistivity of copper, gold, palladium, and silver," *Chem. Ref. Data*, vol. 8, no. 4, p. 1147, 1979. doi: 10.1063/1.555614.

[30] F. Dumas-Bouchiat, C. Champeaux, A. Catherinot, A. Crunteanu, and P. Blondy, "RF-microwave switches based on reversible semiconductor-metal transition of VO_2 thin films synthesized by pulsed-laser deposition," *Appl. Phys. Lett*, vol. 91, no. 22, p. 223,505, 2007. doi: 10.1063/1.2815927.

[31] C. Hillman, P. A. Stupar, J. B. Hacker, Z. Griffith, M. Field, and M. Rodwell, "An ultra-low loss millimeter-wave solid state switch technology based on the metal–insulator – transition of vanadium dioxide," in *Proc. IEEE MTT-S IMS*, Tampa, FL, 2014, pp. 1–4. doi: 10.1109/MWSYM.2014.6848479.

[32] T. T. Wu and R. W. P. King, "The cylindrical antenna with nonreflecting resistive loading," *IEEE Trans. Antennas Propag.*, vol. 13, no. 3, pp. 369–373, May 1965. doi: 10.1109/TAP.1965.1138429.

[33] R. Hansen, "Gain limitations of large antennas: Corrections," *IEEE Trans. Antennas and Propagat.*, vol. 13, no. 6, p. 998, Nov. 1965. doi: 10.1109/TAP.1965.1138538.

[34] D. P. Nyquist and K.-M. Chen, "The traveling-wave linear antenna with non-dissipative loading," *IEEE Trans. Antennas Propag.*, vol. 16, no. 1, pp. 21–31, 1968. doi: 10.1109/TAP.1968.1139113.

[35] F. I. Rial, H. Lorenzo, M. Pereira, and J. Armesto, "Analysis of the emitted wavelet of high-resolution bowtie GPR antennas," *Sensors*, vol. 9, no. 6, pp. 4230–4246, 2009. doi: 10.3390/s90604230.

[36] E. E. Altshuler, "The traveling-wave linear antenna," *IRE Trans. Antennas Propag.*, vol. 9, no. 4, pp. 324–329, July 1961. doi: 10.1109/TAP.1961.1145026.

[37] E. E. Altshuler, "Self- and mutual impedances of traveling-wave linear antennas," *IEEE Trans. Antennas Propag.*, vol. 37, no. 10, pp. 1312–1316, 1989. doi: 10.1109/8.43541.

[38] B. Rama Rao and P. Debroux, "Wideband HF monopole antennas with tapered resistivity loading," in *Proc. IEEE Mil. Com. Conf*, vol. 3. Monterey, CA: IEEE, 1990, pp. 1223–1227. doi: 10.1109/MILCOM.1990.117603.
[39] G. Smith, "Other traveling-wave antennas," Ch. 8, in *An Introduction to Classical Electromagnetic Radiation*, G. Smith, Ed. Cambridge, U.K.: Cambridge Univ. Press, 1997, pp. 546–604.
[40] J.-F. Hofinghoff and L. Overmeyer, "Resistive loaded antenna for ground penetrating radar inside a bottom hole assembly," *IEEE Trans. Antennas Propag.*, vol. 61, no. 12, pp. 6201–6205, Dec. 2013. doi: 10.1109/TAP.2013.2283604.
[41] T. P. Montoya and G. S. Smith, "Vee dipoles with resistive loading for short-pulse ground-penetrating radar," *Microw. Opt. Tech. Lett.*, vol. 13, no. 3, pp. 132–137, Oct. 20, 1996. doi: 10.1002/(SICI)1098-2760(19961020)13:3<132::AID-MOP6>3.0.CO;2-O.
[42] D. Uduwawala, M. Norgren, P. Fuks, and A. W. Gunawardena, "A deep parametric study of resistor-loaded bow-tie antennas for ground-penetrating radar applications using FDTD," *IEEE Trans. Geosci. Remote Sens.*, vol. 42, no. 4, pp. 732–742, Apr. 2004. doi: 10.1109/TGRS.2003.819442.
[43] D. Yanga, J. Panb, Z. Zhaoc, and Z. Nied, "Design of trapezoidal cavity-backed resistance loaded bow tie antenna with ultra-wideband and high directivity," *J. Electromagn. Waves Appl.*, vol. 24, nos. 11–12, pp. 1685–1695, 2010. doi: 10.1163/156939310792149704.
[44] K. Kim and W. R. Scott Jr., "Design and realization of a discretely loaded resistive vee dipole on a printed circuit board," in *Proc. SPIE*, vol. 5089. Bellingham, WA: SPIE, Apr. 2003, pp. 818–829. doi: 10.1117/12.487327.
[45] R. L. Haupt, "Tapered resistive cylindrical parabolic antenna," in *Proc. IEEE AP-S Int. Symp.*, vol. 1. Dallas: IEEE, May 1990, pp. 156–159. doi: 10.1109/APS.1990.115072.
[46] J. Givernaud et al., "Microwave power limiting devices based on the semiconductor–metal transition in vanadium-dioxide thin films," *IEEE Trans. Microw. Theory Techn.*, vol. 58, no. 9, pp. 2352–2361, 2010. doi: 10.1109/TMTT.2010.2057172.
[47] T. Teeslink, D. Torres, J. Ebel, N. Sepúlveda, and D. Anagnostou, "Reconfigurable bowtie antenna using metal-insulator transition in vanadium dioxide," *IEEE Antennas Wireless Propag. Lett.*, vol. 14, pp. 1381–1384, Feb. 2015. doi: 10.1109/LAWP.2015.2407858.
[48] N. Sepúlveda and D. Anagnostou, "Multimedia video of VO_2 patch with resistive heater electrically isolated by a thin SiO_2 layer and increase in temperature (by Joule heating) inducing phase transition, observed by a change in color," IEEE Dataport, 2019. Accessed on: Jan. 16, 2020. [Online]. Available: http://dx.doi.org/10.21227/469r-nj71.
[49] D. Torres et al., "VO_2-based MEMS mirrors", *J. Microelectromech. Syst.*, vol. 25, no. 4, pp. 780–787, 2016. doi: 10.1109/JMEMS.2016.2562609.
[50] D. Anagnostou, M. Chryssomallis, B. Braaten, J. Ebel, and N. Sepulveda, "Reconfigurable UWB antenna with RF-MEMS for on-demand WLAN rejection," *IEEE Trans. Antennas Propag.*, vol. 62, no. 2, pp. 602–608, Feb. 2014. doi: 10.1109/TAP.2013.2293145.
[51] Y. Zhou, X. Chen, C. Ko, Z. Yang, C. Mouli, and S. Ramanathan, "Voltage-triggered ultrafast phase transition in vanadium dioxide switches," *IEEE Electron Dev. Lett.*, vol. 34, no. 2, pp. 220–222, 2013. doi: 10.1109/LED.2012.2229457.
[52] *RG-58*, AW&C, Collegeville, PA. Accessed on: Jan. 26, 2020. [Online]. Available: http://www.awcwire.com/productspec.aspx?id=rg58/u
[53] *RG-59*, AW&C, Collegeville, PA. Accessed on: Jan. 26, 2020. [Online]. Available: http://www.awcwire.com/productspec.aspx?id=rg59/u
[54] *Single Conductor Mil-Spec Wire*, AW&C, Collegeville, PA. Accessed on: Jan. 26, 2020. [Online]. Available: http://www.militarywire.org/singleconductor.htm
[55] "SMA connector series," Amphenol RF, Danbury, CT. Accessed on: Jan. 26, 2020. [Online]. Available: https://www.amphenolrf.com/connectors/sma.html
[56] "Teflon insulated wire and cable specifications," Dacon Systems, Corona, CA. Accessed on: Sept. 2019. [Online]. Available: https://dacon.com/custom-wire-manufacturing/teflon-wire-fep-pfa-etfe/
[57] Diodes Inc. Accessed on: June 2019. [Online]. Available: https://www.diodes.com/assets/Datasheets/products_inactive_data/PAM2303.pdf